

Polarized light coupling to thin silica-air opal films grown by vertical deposition

A. V. Baryshev,* A. B. Khanikaev, R. Fujikawa, H. Uchida, and M. Inoue

Toyohashi University of Technology, Toyohashi, Aichi 441-8580, Japan

(Received 6 March 2007; revised manuscript received 2 May 2007; published 30 July 2007)

Coupling of polarized light to thin silica-air opal films—representatives of high contrast three-dimensional photonic crystals—has been studied in detail. Photonic stop bands were observed in transmission (reflection) spectra and attributed to diffraction from the $\{111\}$ crystallographic planes of the twinned fcc structure. Polarization-resolved transmission spectra manifest a strong anisotropy of light propagation in the films—collapses of stop bands have been demonstrated for the p -polarized light. Reflection spectra of the films under the s -polarized light illumination highlight an unusual behavior of light scattering. Scattered intensity was found to be influenced by multiple Bragg diffraction accompanied by leakage and inflow of energy to major diffraction lobes.

DOI: [10.1103/PhysRevB.76.014305](https://doi.org/10.1103/PhysRevB.76.014305)

PACS number(s): 42.70.Qs, 42.25.Fx, 42.79.Fm

I. INTRODUCTION

There is much research on fabrication and characterization of opal-like three-dimensional photonic crystals (3D PhCs) and inverse structures based on opals. Starting from self-sedimentation driven by gravity—the way to obtain self-assembled synthetic opals, a number of techniques were developed to improve crystalline structure of 3D PhCs composed of spherical particles. Among these techniques are sedimentation at application of external fields and template-directed sedimentation, the Langmuir-Blodgett method, vertical deposition method using flat and patterned substrates, and building of PhCs using nanorobot manipulation (see Ref. 1 and references therein). These 3D PhCs have been designed with the underlying idea that a complete photonic band gap can be opened up in these structures; the situation when the photonic stop bands overlap and form an energy range for electromagnetic waves, which propagation is prohibited irrespective of both the state of polarization and direction in a 3D PhC. Appearance of stop bands in the energy spectra of a PhC is the result of simple and multiple Bragg diffraction of electromagnetic waves from the crystal structure. High dielectric contrast 3D PhCs (or so-called strongly 3D PhCs) and their ideally designed crystalline structure are shown to be key issues responsible for formation of a complete photonic band gap, the inhibition of spontaneous emission and the localization or guiding of light by intentionally introduced defects.²⁻⁴

Despite existence of various representatives of 3D opal-based PhCs, there is a lack of work devoted to evaluation of their crystalline structure by optical means and understanding features of the polarized light coupling to them. From the experimental point of view, it is of great interest to determine evolution of photonic stop bands, amplitudes, and phases of waves diffracted from a PhC, to observe pseudogaps and complete band gaps,⁵ and also to give thorough explanation on connection between these phenomena and diffraction processes in the crystal structure. Recently, experimental results on coupling of differently polarized light to synthetic opals (bulk samples) at the condition of low dielectric contrast have been reported.^{6,7} It is demonstrated that transmissivity (reflectivity, diffraction patterns) changes with the direction

of polarization of incident light, indicating a strong polarization dependence of photonic stop bands of synthetic opals.

The available experimental data on the polarization-resolved study of 3D PhCs at low and high dielectric contrast conditions are incomplete and their interpretation is still ambiguous. According to the authors' knowledge, an experimentally measured photonic band structure (PBS) of 3D opal-based PhCs for nonpolarized light is demonstrated only once.⁸ The polarization- and angle-resolved transmissivity of fcc colloidal crystals are studied along the directions between the L point and the W point.⁹ The results are analyzed in Ref. 10 showing a disagreement between the experimental and calculated spectra. The polarization-resolved reflectivity from the opal-based photonic crystals in the vicinity of the L point of the Brillouin zone (BZ) are studied in Ref. 11. These results provided only the response of the (111) planes originated from simple Bragg diffraction, since spectra were measured in the limited angular range of the incident light.

It is worth mentioning that there is only one report on experimental scanning of the PBS of high contrast PhCs. In 2005, Man *et al.* presented a PBS of 3D photonic quasicrystals.¹² An effective BZ of a sample with complicated icosahedral symmetry was determined, and the PBS of the sample was scanned for linearly independent polarizations of microwaves. However, polarization-dependent features of the PBS of icosahedral quasicrystals remain uncertain. Recently, Istrate *et al.* developed a treatment of light in finite photonic crystals.¹³ The equivalent of the Fresnel coefficients for two-dimensional (2D) PhCs was obtained, and the amplitude and phase of transmitted and reflected waves at interfaces between photonic crystals and homogeneous materials were computed.

Here, we present experimental studies on optical properties of thin silica-air opal films grown using vertical deposition. Angle- and polarization-resolved transmission-reflection spectra show that, for most directions in films, the TM waves couple to film weakly in comparison to the TE ones. Collapses of the TM photonic stop bands were observed when illuminating the films along some directions. Optical spectra allowed comprehensive analysis of crystalline structure of films. Unusual behavior of light coupling to the films, namely bifurcation of reflection peaks and appearance of a double-peak structure, was detected and studied in

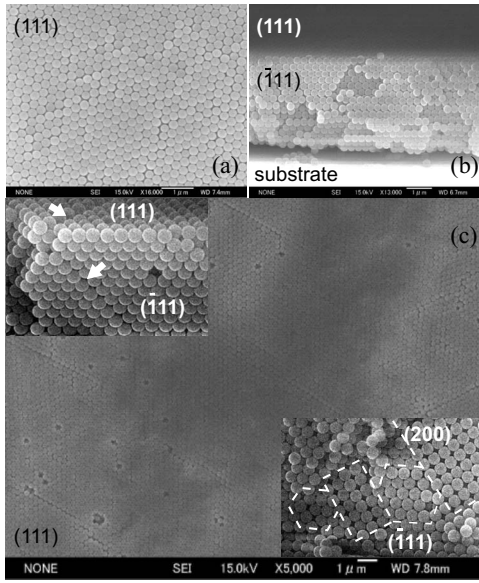


FIG. 1. FESEM images of a thin silica-air opal film. (a) Top view, the (111) plane is oriented parallel to the glass substrate. (b) Edge view, the $(\bar{1}11)$ planes. (c) Large-scale view of junctions between domains; the left-hand inset presents the profile of the junction, the right-hand inset illustrates twinning in films under study.

detail. Experimental spectra indicating this behavior can be found in Refs. 14–16, and theoretical treatment is given in Ref. 17. We offer alternative explanation of this double-peak structure of the specular reflection spectra that is due to multiple Bragg diffraction causing leakage from and inflow of energy to major diffraction lobes. (We would remain that the multiple Bragg scattering is a situation in which two or more Bragg resonances are simultaneously excited in crystal.)

II. EXPERIMENTAL DETAILS

Colloidal α -SiO₂ spheres¹⁸ of diameter of $D \approx 290$ nm suspended in water with density of 1 wt. %, were assembled onto hydrophilic glass substrates using the vertical deposition method. Package of α -SiO₂ spheres and orientation of the layers on the substrate were checked using field emission scanning electron microscopy (FESEM). An opal film grown at these conditions was normally a sequence of about 20 two-dimensional close-packed layers in thickness [the (111) layers in the terms of the fcc lattice, see Figs. 1(a) and 1(c)], which were parallel to the glass substrate [Figs. 1(b) and 2(a)]. FESEM shows that thin silica-air opal films are divided by through-thickness boundaries into domains of different sizes (5–50 μm) [Fig. 1(c)]. Figure 1(b) illustrates a typical cross section of a film; the cleaved edge of the film visualizes a {111}-type plane, the $(\bar{1}11)$ plane hereafter. Figure 1(c) shows a junction of domains, the profile of the junction is seen in the left-hand inset; one can see that the boundary between domains slashes the film. Optical properties of the opal films are confirmed to be governed by the twinned fcc structure with equal volume fraction of twins.¹⁹ The right-hand inset in Fig. 1(c) shows a cleaved edge that ex-

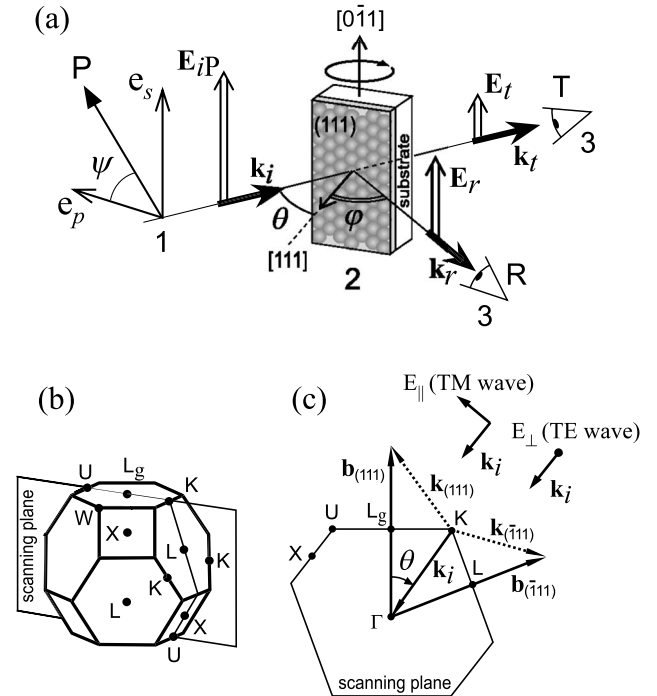


FIG. 2. (a) Schematic of experiments: 1, polarizer; 2, thin silica-air opal film (orientation of chains of spheres is shown); 3, detector. (b) The BZ of the fcc crystal and the scanning plane. (c) The BZ cross section, the L_g - K - L scanning path and a scheme of Bragg diffraction from the {111} planes.

hibits two adjacent domains. One can see the hexagonal and square arrangements of spheres. These arrangements are identical to those for the fcc lattice and visualize the $(\bar{1}11)$ and (200) planes of the growth twins.

Silica-air opal films of different thicknesses were preliminarily tested and were shown to have similar properties. It was found that diffuse scattering increased with rise of film thickness, and stop bands in spectra became less marked especially at large angles of incidence. We selected the films of ~ 20 layers in thickness with pronounced stop bands that were well observable in a wide cone of angles of incidence. To make sure of the inherent structural and optical properties of films grown by vertical deposition, we studied two different films grown at conditions discussed above. Those were sample A—a film subjected to annealing at 750 $^\circ\text{C}$ and an as-grown film—sample B.

Schematic of experiments is shown in Fig. 2. Transmission (reflection) measurements were carried out with the 5-nm spectral resolution using polarized collimated beams (the angle of divergence was less than 1°) from a spectrophotometer (Shimadzu UV-3100), the cross-sectional size of the light beam was about 2 mm². Illuminated area (spot size) on the film surface and the effective optical path in the film under study changed with the angle of incidence, θ . Detected light beams were collected with angular aperture of ≈ 0 (or 5°) by an optical system attached to a motorized rotation stage, in which a lens was focused on the 1.5-mm in diameter entrance window of a light guide. The rotation stage allowed an angular step of $\Delta\varphi = 1^\circ$. To rotate a film about the

vertical axis a holder was used; the sample holder allowed an angular step of $\Delta\theta=0.5^\circ$. When measuring angle-resolved spectra along the L_g - K - L and L_g - W - K paths, the films were rotated about the $[011]$ and $[\bar{1}\bar{1}2]$ axes, respectively [see Fig. 2(a)]. The angle of incidence θ and the angle of detection φ were measured with respect to the normal to the (111) planes. Note that in our experiments samples were aligned so that the beam fell onto opal film and then entered glass substrate. The linearly polarized electric field was adjusted by a polarizer to be of a chosen orientation ($\psi=0^\circ-90^\circ$); where $\psi=90^\circ$ corresponded to the normal \mathbf{E}_\perp component (s polarization), and $\psi=0$ was for the parallel \mathbf{E}_\parallel component (p polarization) to the $L_g\Gamma L$ (or $L_g\Gamma W$) scanning plane. In this work, we use the following notations for light beams with respect to the scanning planes: (i) the s (p) polarization and the \mathbf{E}_\perp (\mathbf{E}_\parallel) electric field for incident light beams, which transmission is denoted as \mathbf{T}_\perp (\mathbf{T}_\parallel), (ii) the \mathbf{E}_ψ polarization is used to tag the plane of polarization chosen by the polarizer, and (iii) the TE (TM) waves for denoting the polarization of beams propagating inside the opal film.

III. RESULTS AND DISCUSSION

In this section, we consider angle- and polarization-resolved transmission spectra for the scanning in the $L_g\Gamma L$ plane (the L_g - K - L path). In the range of $\lambda=370-820$ nm, features in these spectra are originated by a smaller number of lattice planes and show general features of light coupling to silica-air opal films. As for spectra measured at the L_g - W - K scanning, we will refer to these spectra pointing out similarities and differences between them and the spectra measured along the L_g - K - L path. The spectra measured in the vicinity of the W point will be discussed in more detail in Sec. III B.

A. Angle- and polarization-resolved transmissivity

The series of transmission spectra for two opal films are shown in Figs. 3 (sample A) and 4 (sample B). Plots (a) and (b) present the T_\perp and T_\parallel spectra for the s - and p -polarized light, respectively, when scanning films along the L_g - K - L (Fig. 3) and L_g - W - K paths (Fig. 4). The most pronounced resonances were found to be due to Bragg diffraction from $\{111\}$ planes. At normal incidence onto sample A ($\theta=0$, the L_g point, see Fig. 3), transmission spectra for both polarizations show a single Bragg resonance of equal intensity, which is the (111) stop band. In scanning from the L_g point to the L point ($\theta>0$), we found the following results. First, the (111) stop band shifts to the short-wavelength spectral range and another deep, which is defined as the $(\bar{1}\bar{1}\bar{1})$ stop band, experiences the long-wavelength shift. The mentioned spectral shifts are more obvious in plot (a), for the s -polarized light. Note that since the $L_g\Gamma L$ scanning plane is orthogonal to the (111) and $(\bar{1}\bar{1}\bar{1})$ planes, light with the s (p) polarization is the TE (TM) wave when coupling to the (111) and $(\bar{1}\bar{1}\bar{1})$ planes. For the TE waves, the spectral width of the (111) stop band was found to be >45 nm (it has maximal width of 70 nm at $\theta=0$). Width of the $(\bar{1}\bar{1}\bar{1})$ stop band

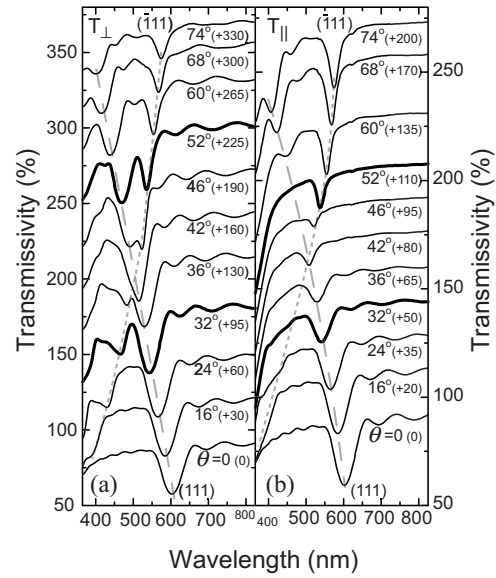


FIG. 3. Transmission spectra measured along the L_g - K - L path on the BZ surface of the fcc lattice: illumination with the s - (a) and p -polarized light (b). Thick lines are for the critical angles; collapses of the stop bands are seen in plot (b). Dashed gray lines are to show spectral shifts of stop bands. The external angle of incidence θ and vertical shifts of transmission spectra are given. (Sample A was used.)

changed from ≈ 20 nm at intermediate angles of $\theta \in [36^\circ; 46^\circ]$ to ≈ 40 nm at other angles.

Second, the transmission of the TE Bragg modes diffracted from the (111) planes, $T_\perp(\lambda_{(111)})$, gradually decreases as θ rises. The opposite behavior is seen in the spectra for the $(\bar{1}\bar{1}\bar{1})$ stop band, the coupling of the corresponding TE Bragg

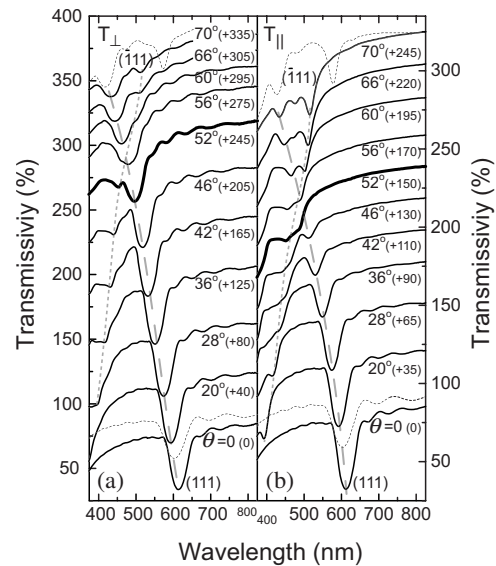


FIG. 4. Transmission spectra measured along the L_g - W - K path on the BZ surface of fcc lattice: illumination with the s - (a) and p -polarized light (b). To make a comparison, thin dashed lines present spectra of sample A; spectra were measured at the same angles of incidence in the $L_g\Gamma L$ scanning plane. (Sample B was used.)

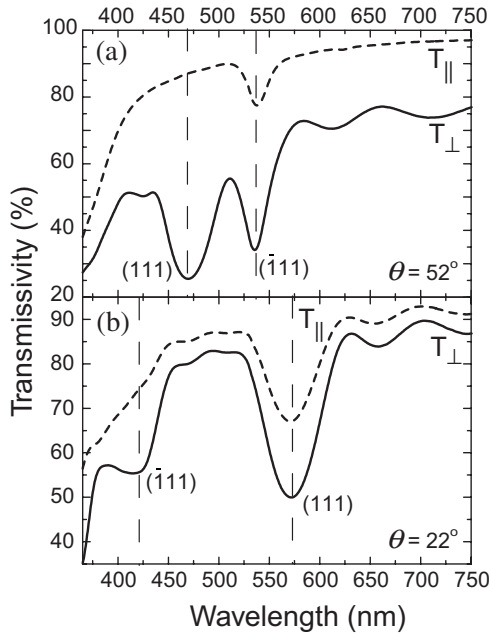


FIG. 5. (Sample A) Comparison of the transmission spectra measured under illumination with the s - and p -polarized light: (a) the (111) stop band does not open for TM waves; (b) the T_{\parallel} spectrum represents the collapse of the $(\bar{1}\bar{1}\bar{1})$ stop band.

modes $[T_{\perp}(\lambda_{(\bar{1}\bar{1}\bar{1})})]$, becomes stronger with rise of θ . Note that as the angle θ increases the smaller becomes the angle of incidence onto the $(\bar{1}\bar{1}\bar{1})$ planes and the longer becomes optical path in the film [i.e., beam passes the larger number of $(\bar{1}\bar{1}\bar{1})$ planes]. This results in increase of intensity of the $(\bar{1}\bar{1}\bar{1})$ stop band.

Third, that is the key finding for high contrast 3D PhCs, the TM Bragg modes propagate throughout the film in sharp contrast to the TE ones. In comparison to the TE modes, the TM light couples to film weakly. Collapses of the TM photonic stop bands were observed, when illuminating the films along specific directions. The (111) stop band weakens with the rise of θ and $T_{\parallel}(\lambda_{(111)})$ gains its maximum at $\theta=52^{\circ}$. At this angle of incidence, the TM wave propagates through the (111) layers without coupling, and the (111) stop band does not open [Fig. 3(b), thick line]. With further rise of $\theta > 52^{\circ}$, the (111) stop band opens and becomes more intensive. Obviously, $\theta=52^{\circ}$ is the Brewster angle, and the effective refractive index ($n_{\text{eff}} \approx 1.28$) of the film under study can be estimated in accord with the Brewster condition, $\theta_B^{(111)} = \arctan(n_{\text{eff}}/n_{\text{air}})$. As for the $(\bar{1}\bar{1}\bar{1})$ stop band, maximal transmissivity of the TM waves in the spectral range corresponding to wavelengths of $\lambda_{(\bar{1}\bar{1}\bar{1})}$ was observed at $\theta=32^{\circ}$. This increase of $T_{\parallel}(\lambda_{(\bar{1}\bar{1}\bar{1})})$ is due to reduction of diffraction efficiency from the (111) planes together with approaching the Brewster condition for the $(\bar{1}\bar{1}\bar{1})$ planes.

Figure 5 depicts pairs of the spectra measured for the s - and p -polarized light. Plots (a) and (b) show the collapse of the (111) and $(\bar{1}\bar{1}\bar{1})$ stop bands for the TM waves, respectively. From Fig. 3(b), it may be seen that determination of the Brewster angle for the $(\bar{1}\bar{1}\bar{1})$ planes is hindered, which is

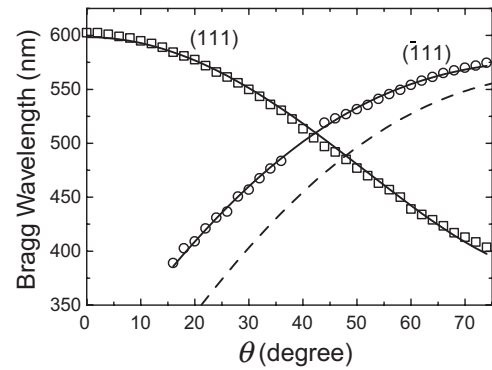


FIG. 6. (Sample A) Experimental (squares and circles) and calculated (solid and dashed lines) spectral positions of stop bands in the T_{\perp} spectra for the L_g - K - L scanning. Dashed line is for the ideal fcc lattice.

most likely because of the short length of the $(\bar{1}\bar{1}\bar{1})$ planes. Transmission spectra show that coupling of the TM waves of $\lambda_{(\bar{1}\bar{1}\bar{1})}$ to the film is negligible for the wide range of angles, $15^{\circ} < \theta < 35^{\circ}$. Results shown in Figs. 3–5 are in agreement with those demonstrated in Refs. 6 and 7 and show that the features in the polarization-resolved transmission spectra can be discussed in terms of Brewster's law and Fresnel reflection with the account of 3D structure of opal films.

Figure 6 illustrates spectral shifts of the observed stop bands of sample A. Shift of the (111) stop band is fitted well by simple Bragg diffraction taking into account refraction on the film surface, $\lambda_{(111)} = 2d_{(111)}n_{\text{eff}} \cos\{\arcsin(\frac{1}{n_{\text{eff}}}\sin\theta)\}$. The effective refractive index n_{eff} of the film is found to be ≈ 1.286 , and the interplanar distance between the (111) planes in the fcc structure $d_{(111)}$ is ≈ 233 nm. Values extracted from the fitting are in good agreement with those evaluated for the film using the Brewster condition (refractive index, $n_{\text{eff}} \approx 1.28$) and from FESEM images (interplanar distance of $d_{(111)} = 0.8165D \approx 236$ nm, where D coincides with the technical data on the purchased α - SiO_2 spheres¹⁸). On the contrary, shift of the $(\bar{1}\bar{1}\bar{1})$ stop band is not fitted with the Bragg condition for the ideal fcc structure (dashed curve in Fig. 6): $\lambda_{(\bar{1}\bar{1}\bar{1})} = 2d_{(\bar{1}\bar{1}\bar{1})}n_{\text{eff}} \cos\{\alpha - \arcsin(\frac{1}{n_{\text{eff}}}\sin\theta)\}$, where $\alpha = 70.5^{\circ}$ is the angle between the (111) and $(\bar{1}\bar{1}\bar{1})$ planes. By fixing the refractive index ($n_{\text{eff}} = 1.286$) and interplanar distance $d_{(\bar{1}\bar{1}\bar{1})} = 233$ nm, the experimentally measured spectral positions of the $(\bar{1}\bar{1}\bar{1})$ stop band are well fitted with Bragg's law for a distorted fcc structure in which α is of $\approx 63^{\circ}$. (When varying both $d_{(\bar{1}\bar{1}\bar{1})}$ and α at fixed n_{eff} , the best fitting provides $d_{(\bar{1}\bar{1}\bar{1})} \approx 228$ nm and $\alpha \approx 61.2^{\circ}$.) Angle α extracted from fitting is a little smaller than that expected for the {111} family in the close-packed fcc structure. It is most likely that this difference is due to the presence of the growth anisotropy influenced by gravity and evaporation acting on assembling α - SiO_2 spheres. However, such deviation from Bragg's law for ideal fcc may also arise in our attempt to find a good fit of spectral shift of the $(\bar{1}\bar{1}\bar{1})$ stop band caused by the extremely limited (~ 20 spheres) extent of the $(\bar{1}\bar{1}\bar{1})$ planes. Care should be taken with the fact that the structure under

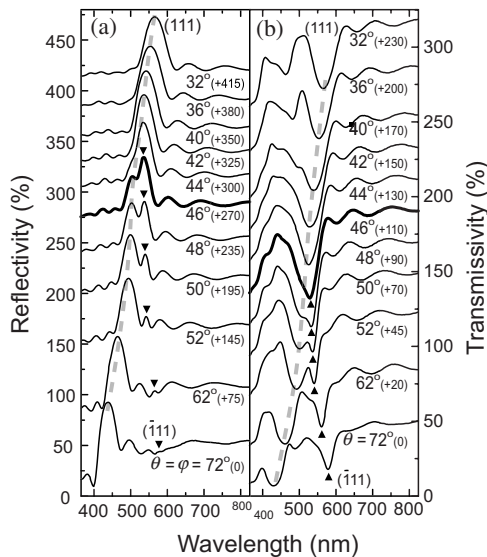


FIG. 7. (Sample A) Angle-resolved reflection (a) and transmission (b) spectra for the s polarization. The spectra are measured along the scanning path $32^\circ < \theta < 72^\circ$ in the $L_g\Gamma K$ scanning plane. Spectral positions of the $(\bar{1}11)$ stop bands are marked by triangles. Spectra corresponding to the most pronounced double-peak structure are given in plots (a) and (b) by the thick line. Angles of incidence (and detection) and shifts are given for each spectrum.

study cannot be treated as a crystal possessing truly 3D crystalline structure. Thin films may be characterized as a 2D +1 photonic quasicrystal, and diffraction processes may be influenced by 2D periodicity of the (111) layers.

Figure 4 shows spectral shifts of the $\{111\}$ stop bands with change of the incident angle and their evolution with direction of polarization, when scanning in the $L_g\Gamma W$ plane. Since the $L_g\Gamma W$ plane is not orthogonal to the $(\bar{1}11)$ planes, the incident s - (p -) polarized light splits into the $TE_{(\bar{1}11)}$ and $TM_{(\bar{1}11)}$ modes with respect to the $(\bar{1}11)$ planes. In this case, the $(\bar{1}11)$ planes can largely reflect the \mathbf{E}_{\parallel} -polarized light (Fig. 4, $\theta > 60^\circ$). Even though the (111) stop bands of sample B are stronger (see Fig. 4, thin dashed lines are for sample A) and the propagating light beam diffracts from two sets of $(\bar{1}11)$ -like planes (one set corresponds to one fcc domain), the $(\bar{1}11)$ stop bands of sample B at the L_g-W-K scanning are of smaller intensity as compared to those of sample A at the L_g-K-L scanning. This is clearly due to conditions of light incidence upon the L_g-W-K scanning: (i) angle of incidence onto $(\bar{1}11)$ -like planes is larger, and (ii) the direction of polarization with respect to $(\bar{1}11)$ -like planes is not purely TE. (Correlation between intensity of photonic stop bands for bulk opal photonic crystals and the direction of polarization is considered in Refs. 6 and 7.)

B. Angle- and polarization-resolved scattering

Reflection and transmission spectra of sample A are shown in Fig. 7. These angle-dependent spectra were measured for the s -polarized light, and reflected (transmitted)

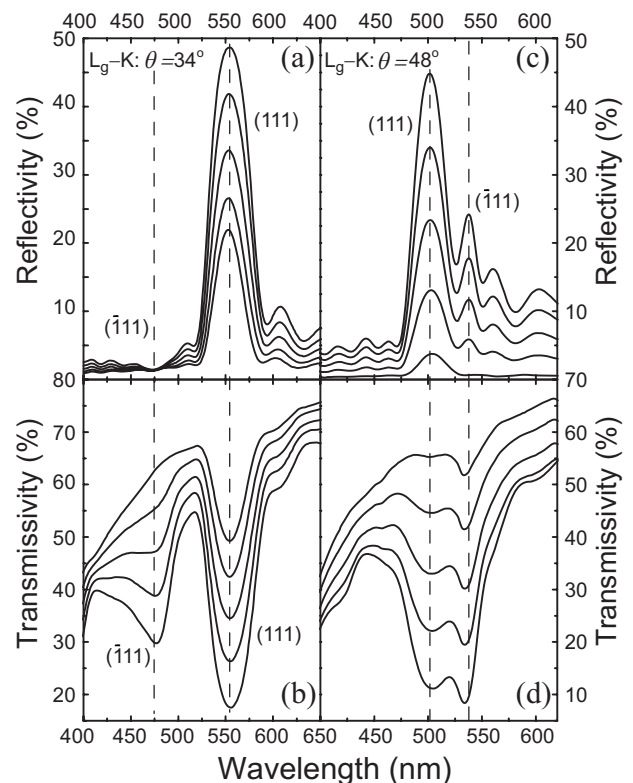


FIG. 8. (Sample B) Sets of spectra measured in specular reflection [(a) and (c)] and transmission configuration [(b) and (d)] at $\theta = 34^\circ$ and 48° (the $L_g\Gamma K$ scanning plane). Stop band with maximal (minimal) intensity corresponds to the \mathbf{E}_{\perp} illumination, $\psi = 90^\circ$ (\mathbf{E}_{\parallel} , $\psi = 0^\circ$); five spectra are shown for $\mathbf{E}_{\psi=0,30,45,60,90}$.

light was collected with the angular aperture of $\approx 5^\circ$. Well-defined single maxima and minima for the (111) Bragg diffraction resonances of practically the same strength may be seen in both reflection and transmission spectra for $\theta < 44^\circ$. Starting from $\theta = 44^\circ$, the spectra of specular reflection ($\varphi = \theta$) bring out an additional feature—the *second peak* is marked by triangle [see plot (a)]. For angles $42^\circ < \theta < 50^\circ$ maxima and minima in the T and R spectra are slightly misaligned. The additional peak in reflection spectra at any angle $\theta > 50^\circ$ has the same spectral position as that in the corresponding transmission spectrum [see plot (b)]. This serves as evidence that these additional peaks are due to diffraction from the $(\bar{1}11)$ planes. However, if the $(\bar{1}11)$ diffraction resonance does exist, this diffracted beam should not be thrown along specular reflection from the film, i.e., from the (111) planes [see Laue conditions in Fig. 2(c)].

To get a thorough insight on the splitting in specular reflection spectra, its evolution in the vicinity of the (111)/ $(\bar{1}11)$ stop-band crossing was measured with the angular step of $\Delta\theta = 0.5^\circ$, using different polarizations and when detecting reflected light with the zero aperture. Sample B was used in these experiments. Let us first consider spectra measured so that the (111) and $(\bar{1}11)$ stop bands are relatively far from their crossing. Figure 8 [plots (a) and (b)] shows sets of spectra measured in specular reflection and transmission geometries at $\theta = 34^\circ$. Stop band with maximal and minimal intensity corresponds to the \mathbf{E}_{\perp} ($\psi = 90^\circ$, s po-

larization) and E_{\parallel} ($\psi=0$, p polarization) illumination, respectively; five spectra are shown for $E_{\psi=0,30^\circ,45^\circ,60^\circ,90^\circ}$ in each plot. It is evident that spectral positions of peaks in reflection and transmission spectra coincide (see dashed lines). The (111) and $(\bar{1}\bar{1}\bar{1})$ stop bands are well aligned when changing the direction of polarization. This is also illustrated in plots (c) and (d). As for the correlation between intensities of stop bands in plots (a) and (b), a weak leakage of energy was observed in the reflection spectra ($\lambda \approx 475$ nm). The $(\bar{1}\bar{1}\bar{1})$ stop band is well defined in the transmission spectrum and introduces the shallow band in the reflection spectrum. Sets of spectra presented in plots (c) and (d) were measured at $\theta=48^\circ$ for different polarizations on analogy with those discussed above. In this case, one can see a slight misalignment of spectral positions of peaks in reflection and transmission spectra for the $(\bar{1}\bar{1}\bar{1})$ resonance; meanwhile, the resonances in spectra do not shift when changing the direction of polarization. On the contrary to the case of $\theta=34^\circ$, the light beam diffracted from the $(\bar{1}\bar{1}\bar{1})$ planes inflows to specular reflection from the film [i.e., from the (111) planes] and has an appreciable intensity. Clearly, intensity of the $(\bar{1}\bar{1}\bar{1})$ peak depends on strength of the $(\bar{1}\bar{1}\bar{1})$ stop band in transmission spectra. This intensity decreases up to zero when the corresponding band in transmission spectrum weakens but still has nonzero depth. The mentioned difference between intensities in transmission and reflection spectra taken at $\psi_p \neq 0$ indicate that light being diffracted from the $(\bar{1}\bar{1}\bar{1})$ planes is, however, thrown along specular reflection. As for the spectra measured at $\psi=0$ ($\theta=48^\circ$), they indicate that inflow of energy completely ceases, while the $(\bar{1}\bar{1}\bar{1})$ stop band in the transmission spectrum is still observable. Thus, these experiments show two opposite manifestations of the $(\bar{1}\bar{1}\bar{1})$ stop band in reflection spectra—the leakage from and inflow of energy to the direction of specular reflection.

Figure 9 illustrates cases where light coupling results in a most-pronounced double-peak structure of specular reflection spectra [plots (a)–(c) for the K point, plots (d)–(f) for the W point]. These spectra are given by thick lines in plots (a) and (d). To better observe changes in intensity of reflected light in the vicinity of stop-band crossings (i.e., when photonic stop bands converge towards each other), spectra were measured with small angular step. Since experiments were done using the E_{\perp} - and $E_{\psi=60^\circ}$ -polarized light for the K and W points, respectively, one could expect that intensity of the (111) stop band would rise with increased angle θ (in analogy with the Fresnel equation for the s polarization). Spectra in Figs. 3(a), 7(a), and 9(a) demonstrate this tendency for the (111) stop bands while they are spectrally separated from the $(\bar{1}\bar{1}\bar{1})$ stop bands. However, in the vicinity of the K and W points intensity of the (111)-reflected light decreases. This is clearly due to leakage of energy from specular reflection when diffraction conditions are satisfied for two (or more) crystal planes. For the W point, the shape of contour of the (111) stop band changes slightly when crossing with other $\{111\}$ stop bands. Note that the $E_{\psi=60^\circ}$ polarization was chosen to better observe this change. One can distinguish a weak disturbance of the (111) stop band [see plot (d)]. Contrary,

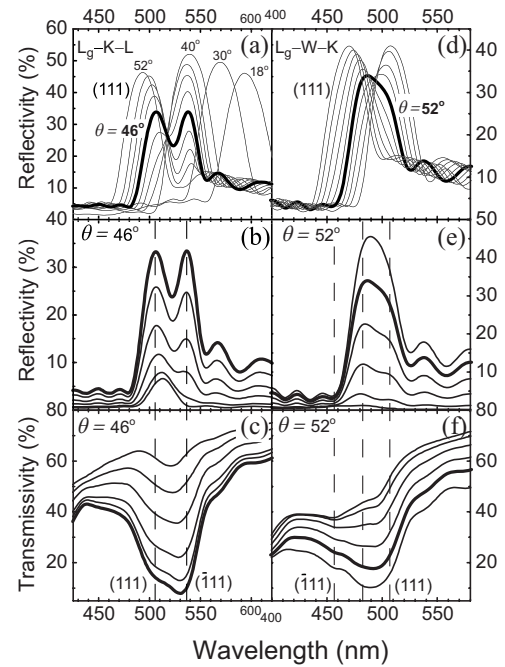


FIG. 9. (Sample B) Sets of spectra measured in specular reflection and transmission configurations for the L_g - K - L scanning: (a) angle-dependent specular reflection of TE waves ($\psi=90^\circ$); (b) reflectivity; and (c) transmissivity at $\theta=\varphi=46^\circ$ —stop band with maximal (minimal) intensity corresponds to the E_{\perp} illumination, $\psi=90^\circ$ (E_{\parallel} , $\psi=0$); six spectra are shown for $E_{\psi=0,15^\circ,30^\circ,45^\circ,60^\circ,90^\circ}$. The L_g - W - K scanning: (d) angle-dependent specular reflection of $E_{\psi=60^\circ}$ waves; (e) reflectivity; and (f) transmissivity at $\theta=\varphi=52^\circ$ —stop band with maximal (minimal) intensity corresponds to the E_{\perp} illumination, $\psi=90^\circ$ (E_{\parallel} , $\psi=0$); six spectra are shown for $E_{\psi=0,15^\circ,30^\circ,45^\circ,60^\circ,90^\circ}$.

the (111) stop band (or reflection spectrum in other words) is strongly affected for the K point [see plot (a)].

In analogy to spectra presented in Fig. 8, transmissivity and reflectivity for the K ($\theta=46^\circ$) and W points ($\theta=52^\circ$) were measured with change of ψ (Fig. 9). One can see that the right peaks in spectra for the K point [plot (b)] are well aligned, while the left ones experience small long-wavelength shift. The right-hand peak collapses but the left-hand one only weakens ($\psi=0$). Thus, this case is very similar to that discussed for $\theta=48^\circ$ [Figs. 8(c) and 8(d)]. As for the W point [plot (e)], intensity of the slightly affected contour of the (111) stop band reduces as a whole; note that two peaks are resolved at $\psi=15^\circ, 30^\circ$, and 45° . One can conclude that contribution of inflow-leakage processes to disturbance of specular reflection spectra is negligible at illumination along the Γ - W direction. The observed difference between spectra for the K and W points is due to the mutual orientation of the film structure and probing light beam. Crossing of stop bands reduces intensity of a Bragg resonance detected in specular reflection geometry, and for the certain experimental geometries, can result in either strong or negligible change of resonance contours. At illumination along the Γ - K direction, specific coupling takes strongest effect on specular reflection (or diffraction) from the (111) planes.

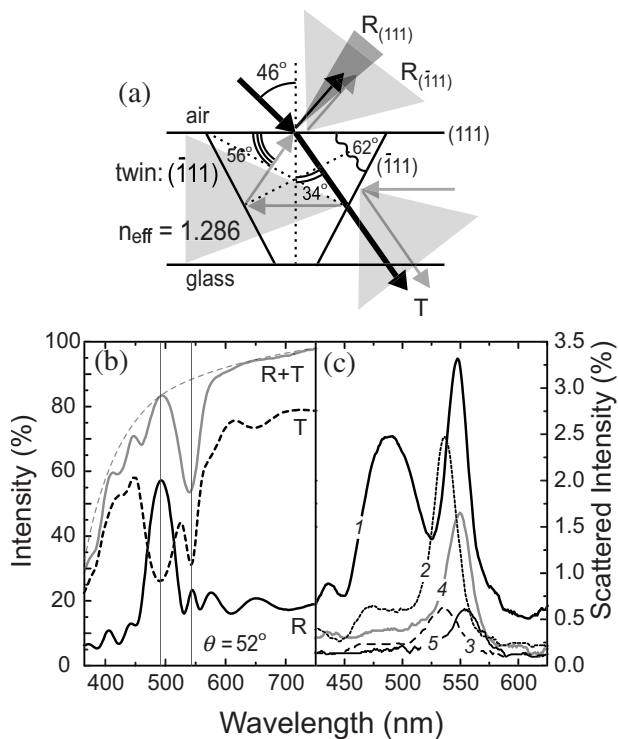


FIG. 10. (a) Schematic of diffraction processes in films at $\theta = 46^\circ$ (the $L_g\Gamma K$ scanning plane). (b) Transmission ($\theta = 52^\circ$) and specular reflection spectra ($\varphi = 52^\circ$), and also their sum for sample A at illumination with the s -polarized light. The thin dashed line is guided to the eye representing an approximate diffuse background of scattering in the film. (c) Spectra of scattered light ($\theta = 52^\circ \neq \varphi$): (1) $\varphi = 46^\circ$, (2) 56° , (3) 40° , (4) 44° , and (5) 60° .

C. Discussion

The diffraction processes causing appearance of the additional $(\bar{1}\bar{1}\bar{1})$ -type maxima in specular reflection spectra can be easily found by considering a scheme of diffraction from the twinned fcc structure [Fig. 10(a)]. Note that angles shown in the scheme meet (i) observation of the most-pronounced double-peak structure of reflection spectra, (ii) fitting presented in Fig. 6, and (iii) the idea that a portion of the $(\bar{1}\bar{1}\bar{1})$ -diffracted light goes along the film at this particular geometry of experiment.

Experimental data presented in Secs. III A and III B are in favor of multiple Bragg diffraction wherein a -SiO₂ spheres scatter resonant wavelengths ($\lambda = 475$ – 575 nm) into four channels. The (111) stop band (diffraction channel 1) in reflection spectra weakens as it converges towards the $(\bar{1}\bar{1}\bar{1})$ resonance (see Figs. 7–9). This is due to the $(\bar{1}\bar{1}\bar{1})$ diffraction (channel 2) [see Laue diagram, Fig. 2(c)] resulting in leakage of energy from specular reflection. [Let us recall again that the film under study has the twinned fcc structure and has mosaic domain structure (see Fig. 1, Ref. 19)]. Bragg resonant light turned by the $(\bar{1}\bar{1}\bar{1})$ planes of twin 1 (channel 2) can propagate along an extended optical path inside the film. Moreover, this light can be guided along the (111) planes [see Fig. 10(a)]. If so, this $(\bar{1}\bar{1}\bar{1})$ -diffracted beam is also reso-

nant for twin 2 due to the mirror symmetry of fcc twins. This beam experiences diffraction from a $\{\bar{1}\bar{1}\bar{1}\}$ plane of twin 2 (channel 3), and then leaves the film. Such diffraction process contributes to the specular reflection and has maximal strength when resonant light is maximally trapped within the film. On the other hand, the $\{\bar{1}\bar{1}\bar{1}\}$ resonant light diffracted from twin 2 must fully compensate the leakage that is due to twin 1. To resolve this ambiguity the following experiment was done.

Figure 10 shows spectra measured in transmission ($\theta = 52^\circ$, the $L_g\Gamma K$ scanning plane) and specular reflection geometries ($\theta = \varphi = 52^\circ$), their sum [plot (b)] and spectra of light scattering ($\theta = 52^\circ \neq \varphi$) [plot (c)]. One can see that the sum of the R and T spectra (gray solid line) behaves in a different way at wavelengths corresponding to the (111) and $(\bar{1}\bar{1}\bar{1})$ peaks. A sharp minimum in the $R+T$ spectrum is seen at $\lambda_{(\bar{1}\bar{1}\bar{1})} = 540$ nm, which corresponds to spectral position of the $(\bar{1}\bar{1}\bar{1})$ stop band. As for the relationship between reflectivity and transmissivity at $\lambda_{(111)} = 490$ nm, there is not any minimum in the $R+T$ spectrum. The latter means that the reflected and transmitted waves of $\lambda_{(111)} = 490$ nm complement each other with account of diffuse scattering. Contrary, for the $(\bar{1}\bar{1}\bar{1})$ diffraction process there is no quantitative agreement between the $R(\theta = \varphi = 52^\circ)$ and $T(\theta = 52^\circ)$ spectra. Plot (c) shows a set of spectra measured with change of the detection angle ($\varphi \neq 52^\circ$). These spectra bring out characteristic features for both diffraction processes. The (111) planes are extended on the scale of tens of microns in both twins, that is why an angular cone of the (111) diffraction is narrowly directed (diffracted light is not detected at small detector's departure from $\varphi = 52^\circ$), and the maximal intensity is detected along the specular reflection direction. Second, the $(\bar{1}\bar{1}\bar{1})$ resonant light is spread in a wide angular cone, it out-comes from the sample with different amplitudes, and the maximal scattered intensity was also detected in the specular geometry. It is most likely that the short extent of the $(\bar{1}\bar{1}\bar{1})$ planes together with twinning in films on the micron scale are responsible for the spread cone of diffraction. The short extent of the $(\bar{1}\bar{1}\bar{1})$ planes is also liable for the spectral width and intensity of the $(\bar{1}\bar{1}\bar{1})$ stop band. They increase as the angle of light incidence onto $(\bar{1}\bar{1}\bar{1})$ planes decreases; in this case, light beam passes more $(\bar{1}\bar{1}\bar{1})$ planes (see Figs. 3 and 4). Surely, collecting signal in the specular reflection geometry allows to detect only a portion of the $\{\bar{1}\bar{1}\bar{1}\}$ -diffracted light, so the $R+T$ spectrum has minimum at $\lambda_{(\bar{1}\bar{1}\bar{1})}$.

To answer the question “why both peaks may have the same intensity in specular reflection spectra for the K point,” the following complementary processes can be suggested. First, multiple Bragg diffraction causes bouncing the resonant light between the (111) planes together with its coupling to a large possible number of fcc domains when the $(\bar{1}\bar{1}\bar{1})$ diffracted from twin 1 light of the same wavelengths propagates perpendicular to the $[111]$ direction. Second, the reflection from the interfaces between film and air (film and glass substrate) can produce additional scattering processes so that

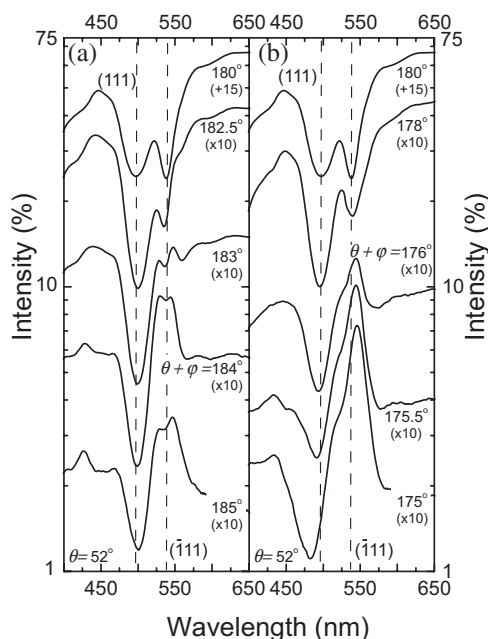


FIG. 11. Spectra of attenuation and inflow of the $\{111\}$ diffracted light to the direction of detection ($\theta=52^\circ$, $\theta+\varphi=180\pm 5^\circ$). Angle of detection for each spectrum is shown; vertical shift and its operator are given in parentheses. Sample B was illuminated with the s -polarized light (the $L_g\Gamma K$ scanning plane).

twin 2 acts in full analogy to twin 1. The suggested processes largely couple the (111) resonant light out of specular reflection. This brings strong reduction of the diffraction contour intensity [see Figs. 9(a) and 9(d)]. As for the double-peak structure, we may assume that there are two portions of the $(\bar{1}\bar{1}1)$ -diffracted light that are leaking and inflowing modes. They both influence the diffraction contour shape, and an intensity ratio between them governs actual strength of peaks.

The presence of a $(\bar{1}\bar{1}1)$ -diffracted light propagating perpendicular to the $[111]$ direction, i.e., along opal films, can be detected when analyzing scattered light intensity behind films in directions which are close to the optical transmission line ($\theta+\varphi=180\pm 5^\circ$, the $L_g\Gamma K$ scanning plane). Figure 11 shows results of this experiment ($\theta=52^\circ$). One can see that the resonant wavelengths $\lambda_{(111)}$ and $\lambda_{(\bar{1}\bar{1}1)}$ leave the sample in a different way. Light diffracted from the (111) planes is always attenuated; the (111) dip is seen in all spectra. Contrary, the $(\bar{1}\bar{1}1)$ -diffracted light experiences both attenuation and strengthening (see minima and cusps centered at $\lambda_{(\bar{1}\bar{1}1)}$). Light flow directions and cones of diffraction are given in

gray in Fig. 10(a). The observed strengthening is due to the fourth diffraction process (Bragg diffraction from twin 1) inflowing into the optical transmission line.

IV. CONCLUSION

Optical properties of samples under our study were shown to reflect intrinsic structure of thin silica-air opal films grown onto glass substrates under vertical deposition conditions. Data on polarized light coupling to the films provided background knowledge of their structural and dielectric properties. Structure of the films was found to be the twinned fcc. Spectra measured in transmission and reflection geometries allowed to study in detail Bragg diffraction processes taking place in the films. Collapses of the $\{111\}$ stop bands for the TM waves propagating in high contrast 3D PhCs were observed. These results provide convincing experimental evidence that the TM waves do not couple to PhCs, when propagating along critical directions, and have destructive effect on formation of complete band gaps. Polarization-dependent features of spectra can be qualitatively understood by analogy with Fresnel reflection and Brewster's effect.

Experiments using the s -polarized light were shown to be essential for studies on structural properties of thin silica-air opal films. They allowed demonstrating all the Bragg diffraction processes taking place in the film structure. Despite extremely small extent of the $(\bar{1}\bar{1}1)$ planes, their contribution to multiple Bragg diffraction is irrefutable. When interacting with an opal film, an incident light beam of a particular wavelength can experience multiple Bragg diffraction that goes simultaneously into several channels. Intensities and contours of stop bands in specular reflection spectra were found to decrease and to have the pronounced double structure, respectively, when the (111) and $(\bar{1}\bar{1}1)$ stop bands converge towards each other. In these particular geometries the incident light beam diffracts so that it propagates along the films, i.e., becomes an in- (111) -plane guided wave. The observed light guiding mechanism due to diffraction from crystallographic planes in 3D structures may have benefits for excitation of waveguide modes and multidirectional guidance.

ACKNOWLEDGMENTS

The authors are grateful to A. V. Sel'kin, A. B. Granovsky, and A. A. Fedyanin for helpful discussions. This work was supported in part by the super optical information memory project by MEXT, Grant-in-Aid for Scientific Research from JSPS (No. 17106004), Japan.

*Permanent address: A. F. Ioffe Physico-Technical Institute, St. Petersburg, Russia.

¹C. Lopez, *Adv. Mater.* (Weinheim, Ger.) **15**, 1679 (2003).

²J. D. Joannopoulos, R. D. Meade, and J. N. Winn, *Photonic Crystals* (Princeton University Press, Princeton, NJ, 1995).

³E. Yablonovitch, *Phys. Rev. Lett.* **58**, 2059 (1987); E. Yablonovitch and T. J. Gmitter, *ibid.* **63**, 1950 (1989).

⁴S. John, *Phys. Rev. Lett.* **58**, 2486 (1987).

⁵K. Busch and S. John, *Phys. Rev. E* **58**, 3896 (1998).

⁶A. V. Baryshev, A. B. Khanikaev, H. Uchida, M. Inoue, and M. F.

- Limonov, Phys. Rev. B **73**, 033103 (2006).
- ⁷M. V. Rybin, A. V. Baryshev, M. Inoue, A. A. Kaplyanskii, V. A. Kosobukin, M. F. Limonov, A. K. Samusev, and A. V. Sel'kin, Photonics Nanostruct. Fundam. Appl. **4**, 146 (2006).
- ⁸A. V. Baryshev, A. A. Kaplyanskii, V. A. Kosobukin, K. B. Samusev, D. E. Usvyat, and M. F. Limonov, Phys. Rev. B **70**, 113104 (2004).
- ⁹I. I. Tarhan and G. H. Watson, Phys. Rev. Lett. **76**, 315 (1996).
- ¹⁰V. Yannopoulos, N. Stefanou, and A. Modinos, J. Phys.: Condens. Matter **9**, 10261 (1997).
- ¹¹J. F. Galisteo-Lopez, F. Lopez-Tejiera, S. Rubio, C. Lopez, and J. Sanchez-Dehesa, Appl. Phys. Lett. **82**, 4068 (2003).
- ¹²W. Man, M. Menges, P. J. Steinhard, and P. M. Chaikin, Nature (London) **436**, 993 (2005).
- ¹³E. Istrate, A. A. Green, and E. H. Sargent, Phys. Rev. B **71**, 195122 (2005).
- ¹⁴H. M. vanDriel and W. L. Vos, Phys. Rev. B **62**, 9872 (2000).
- ¹⁵S. G. Romanov, T. Maka, C. M. Sotomayor Torres, M. Muller, R. Zentel, D. Cassagne, J. Manzanares-Martinez, and C. Jouanin, Phys. Rev. E **63**, 056603 (2001).
- ¹⁶J. F. Galisteo-Lopez, E. Palacios-Lidon, E. Castillo-Martinez, and C. Lopez, Phys. Rev. B **68**, 115109 (2003).
- ¹⁷A. V. Sel'kin, Proceedings of the 12th International Symposium on Nanostructures: Physics and Technology, 2004, pp. 111–112; A. V. Sel'kin, A. Yu. Bilibin, A. Yu. Men'shikova, Yu. A. Pashkov, N. N. Shevchenko, and A. G. Bazanova, Bull. Russ. Acad. Sci. Phys. **68**, 1111 (2005).
- ¹⁸Spheres were purchased from Nippon Shokubai Co.
- ¹⁹R. Fujikawa, A. V. Baryshev, K. Nishimura, H. Uchida, and M. Inoue, J. Porous Mater. **13**, 287 (2006).